In-situ growth of nonstoichiometric CrO0.87 and Co3O4 hybrid system for the enhanced electrocatalytic water splitting in alkaline media

Muhammad Yameen Solangi, Umair Aftab, Aneela Tahira, Abdul Hanan, Monica Montecchi, Luca Pasquali, Matteo Tonezzer, Raffaello Mazzaro, Vittorio Morandi, Abdul Jaleel Laghari, et al.

In-situ growth of nonstoichiometric $CrO_{0.87}$ and Co_3O_4 hybrid system for the enhanced electrocatalytic water splitting in alkaline media

Muhammad Yameen Solangi[a], Umair aftab[a], Aneela Tahira[c], Abdul Hanan[d], Monica Montecchi[f], Luca Pasquali[g.h.i], Matteo Tonezzer[L], Raffaello Mazzaro[e], Vittorio Morandi[e], Abdul Jaleel Laghari[a], Ayman Nafady[k], Muhammad Ishaq Abro[a], Melanie Emo[j], Brigitte Vigolo[j], Elmuez Dawi[m], Elfatih Mustafa[n], and Zafar Hussain Ibupoto[b].

[a]Department of Metallurgy and Materials Engineering, Mehran University of Engineering and Technology, 76080, Jamshoro, Pakistan.

[b]Dr M. A. Kazi Institute of Chemistry University of Sindh, Jamshoro, 76080, Pakistan.

[a]Institute of Chemistry, Shah Abdul Latif University Khairpur Mirs, Sindh, Pakistan.

[d]Key Laboratory of Superlight Material and Surface Technology, Ministry of Education, College of Materials Science and Chemical Engineering, Harbin Engineering University, 150001, Harbin, PR China.

[e]Department of science and technology, CNR IMM, Bologna, Italy.

[f]Engineering Department, University of Modena and Reggio Emilia, Modena, Italy.

[g]Engineering Department, University of Modena and Reggio Emilia, Modena, Italy.

[h]Chemistry, IOM-CNR Institute, Trieste, Italy.

[i]Department of Physics, University of Johannesburg, Auckland Park, South Africa.

[j]Université de Lorraine, CNRS, IJL, F-54000 Nancy, France.

[k]Department of Chemistry, College of Science, King Saud University, Riyadh 11451, Saudi Arabia.

[L]MEM-CNR, Sede di Trento-FBK, Trento, Italy.

[m]Nonlinear Dynamics Research Center (NDRC), Ajman University, Ajman, P.O. Box 346, United Arab Emirates.

[n]Department of Science and Technology (ITN), Linköping University, Campus Norrköping, 601 74, Norrköping, Sweden.

[*]**Corresponding author (s):** Zafar Hussain Ibupoto

E-mail: zaffar.ibhupoto@usindh.edu.pk

Abstract

The development of electrocatalysts for electrochemical water splitting has received considerable attention in response to the growing demand for renewable energy sources and environmental concerns. In this study, a simple hydrothermal growth approach was developed for the in-situ growth of non-stoichiometric $CrO_{0.87}$ and Co_3O_4 hybrid materials. It is apparent that the morphology of the prepared material shows a heterogeneous aggregate of irregularly shaped nanoparticles. Both $CrO_{0.87}$ and Co_3O_4 have cubic crystal structures. Its chemical composition was governed by the presence of Co, Cr, and O as its main constituents. For understanding the role $CrO_{0.87}$ plays in the half-cell oxygen evolution reaction (OER) in alkaline conditions, $CrO_{0.87}$ was optimized into Co_3O_4 nanostructures. The hybrid material with the highest concentration of $CrO_{0.87}$ was found to be highly efficient at driving OER reactions at 255 mV and 20 mA cm^{-2}. The optimized material demonstrated excellent durability for 45 hours and a Tafel slope of 56 mV dec^{-1}. Several factors may explain the outstanding performance of $CrO_{0.87}$ and Co_3O_4 hybrid materials, including multiple metallic oxidation states, tailored surface properties, fast charge transport, and surface defects. An alternative method is proposed for the preparation of new generations of electrocatalysts for the conversion and storage of energy.

Keywords: Nonstoichiometric growth, $CrO_{0.87}$ and Co_3O_4 hybrid material, oxygen evolution reaction

1. Introduction

Global warming, the loss of natural energy resources, the growth of civilizations, and the industrialization of the world have all contributed to the energy crisis that has been recognized as a major problem for the survival of life on earth [1-3]. Fossil fuel production is considered a perilous issue because of the depletion of fossil resources and the generation of toxic pollutants harmful to the earth's ecosystem [4, 5]. As a solution to these issues, the world is demanding renewable energy that has the characteristics of green fuels and produces no pollution of the environment [6, 7]. Based on this perspective, hydrogen energy represents an attractive energy source for sustainable energy production and the rapid development of fuel cell technology. In

comparison to other renewable energy sources, hydrogen energy consists of hydrogen gas fuel which carries the greatest density of energy per unit mass [8-11]. A method of electrochemical water splitting followed by two reactions, namely the hydrogen evolution reaction (HER) and the oxygen evolution reaction (OER). [12-16]. The generation of hydrogen energy from water splitting is potentially cost-effective, if highly efficient nonprecious electrocatalysts are developed in the near future, as precious metal electrocatalysts have been used to date. However, the lack of efficient non-noble electrocatalysts renders hydrogen production impossible [17-19]. The main challenge for hydrogen energy production from water splitting is the slow kinetics of the OER reaction as it occurs by the four electron transfer mechanism [20-22]. Thus, noble metal based electrocatalysts such as iridium oxide (IrO_2) and ruthenium oxide (RuO_2) have been utilized as catalysts in OER reactions, but their high cost and limited availability have limited their application to large-scale water splitting [23-25]. In light of these circumstances, researchers are focusing on the development of nonprecious electrocatalysts based on transition metal compounds in light of their abundance, low cost of fabrication, and significant effectiveness for the OER reaction [26-29]. Several transition metal-based catalysts have been investigated, including metal phosphide, metal selenide, metal sulfide, bimetallic sulfide, metal oxide, bimetallic oxide, and trimetallic oxide [30-38]. As a result of their enhanced electrocatalytic properties, metal oxides (Co, Ni, Mn, Mg, and Fe, for example) tend to be preferred among these catalysts [39-43]. The cobalt based electrocatalyst including Co_3O_4 [44], Co_3O_4-P [45], Ni-Co_3O_4 [46], Mg-Co_3O_4 [47], CdO-Co_3O_4 [48], Fe_3O_4/Co_3O_4 [49], and MgO@Co_3O_4 [50] etc. are widely reported owing to their significant corrosion resistance in alkaline media, high active sites and cost effective fabrication process [51, 52].

This nanostructured catalyst, however, exhibits a large overpotential for OER reactions and consumes a significant amount of potential during the reaction. Thus, it is highly imperative to develop a new generation of electrocatalysts based on Co_3O_4 that can fully satisfy the requirements for electrocatalytic properties for water splitting. In our review of the literature, we find that there has been no study or effort made to develop a non-stoichiometric hybrid electrocatalyst for efficient OER half-cell water splitting based on chromium oxide ($CrO_{0.87}$) and Co_3O_4. Under alkaline conditions, $CrO_{0.87}$ has abundant catalytic sites and chemical states that could support the creation of surface vacancies, and enhance the performance of Co_3O_4 with respect to active OER.

As part of this study, we utilized a simple and low-cost approach for developing in situ heterogeneous electrocatalysts based on $CrO_{0.87}$ and Co_3O_4 using a hydrothermal method. Different analytical techniques were employed to study the morphology, surface chemical composition, and crystal quality of the hybrid $CrO_{0.87}$ and Co_3O_4 material. XRD and XPS tests demonstrated that a hybrid material based on $CrO_{0.87}$ and Co_3O_4 had been successfully formed. In the present study, the hybrid material was used as an efficient OER electrocatalyst that drove the reaction with a low overpotential and was highly durable at different densities of current.

2. Experimental work

2.1. Materials

Potassium chromate ($K_2\ CrO_4$), cobalt chloride hexahydrate ($CoCl_2.6H_2O$), urea ($CH_4\ N_2\ O$), Nafion (5 wt%), 20% RuO_2/C, sodium hydroxide (NaOH) and potassium hydroxide (KOH) were received from Sigma Aldrich, Karachi, Sindh Pakistan. The chemical components were of high analytical grade and utilized without any further preprocessing. Growth and electrolytic solutions were prepared in deionized water.

2.2. Synthesis of $CrO_{0.87}$ and Co_3O_4 hybrid material

Hybrid materials are typically synthesized in the following manner:

Hydrothermal treatment of cobalt chloride hexahydrate and urea in 100 mL of deionized water was used to prepare the cobalt precursors. For the in situ growth of $CrO_{0.87}$ and Co_3O_4 hybrid material, 0.1 g, 0.2 g, and 0.3 g of potassium chromate were mixed with the cobalt precursors and labeled CCR-0.1, CCR-0.2, and CCR-0.3, respectively. Potassium chromate was mechanically stirred for 30 minutes in a highly acidic growth solution. Therefore, we adjusted the pH of growth solutions to 7.5 by adding 0.2 M NaOH. The growth solutions were covered with a thin aluminum sheet to prevent spoilage. The hydrothermal process was conducted in an electric oven at 95^0 C for five hours. In the event that the growth time and cooling to room temperature have been completed, the prepared samples will be removed from the electric oven. A fine powder of the grown material was collected through filter paper in a China dish and washed several times with deionized water. The samples were dried in an electric oven at 65^0 C for four hours, and we were able to obtain a hybrid material based on cobalt hydroxide. Additionally, the samples were thermally burned in an electric furnace at 500°C for 5 hours to convert the hydroxide phase into the oxide phase. Having completed the calcination process and

reached room temperature, samples were removed from the electric furnace. In this regard, we were able to achieve a number of $CrO_{0.87}$ and Co_3O_4 hybrid materials, which were then used for a variety of characterizations, such as structural and functional studies. It was also possible to prepare pristine samples of $CrO_{0.87}$ and Co_3O_4 by the same method in the absence of potassium chromate in order to understand the role of the desired hypothesis. Schematic 1 illustrates the growth process as a stepwise process.

2.3. Physical Characterization $CrO_{0.87}$ and Co_3O_4 hybrid materials

ZEISS Gemini SEM 500 equipped with a field emission gun was used to perform scanning electron microscopy (SEM). The X-ray diffractograms were recorded through Bruker D8 Advance diffractometer with source CuKα radiation having a wavelength of 1.54050 Å, operated at 45 mA and 45 kV, for the determination of phase purity and crystal quality of material. FTIR-PerkinElmer Spectrum Two was used to perform Fourier transform infrared spectroscopy to validate the interaction between $CrO_{0.87}$ and Co_3O_4 in the 400 cm-1 to 4000 cm^{-1} region.

2.4. Half-cell OER measurements on the $CrO_{0.87}$ and Co_3O_4

Measurements of the OER were carried out using the Potentiostat Model VERSASTAT4-500, which consists of a silver-silver chloride (Ag/AgCl) reference electrode, a platinum (Pt) wire counter electrode, and a glassy carbon electrode (GCE) as a working electrode. Initially, catalyst ink solutions of different samples of $CrO_{0.87}$ and Co_3O_4 were prepared by mixing 5 mg of each sample in 1 mL of deionized water accompanied by the addition of 20 µL of Nafion (5 wt.%). GCEs were cleaned properly by polishing silicon paper and alumina slurry. The ink was then modified by drop casting with the prepared catalyst ink. An oxygen evolution reaction (OER) was analyzed using linear sweep voltammetry (LSV) in 1.0 M KOH electrolyte at a scan rate of 1 mV/s. An electrochemical active surface area (ECSA) was calculated based on cyclic voltammetry (CV) of electrocatalysts recorded for non-Faradic regions at different scan rates. In order to determine the charge transport characteristics of various catalytic materials, electrochemical impedance spectroscopy (EIS) was applied at onset OER potential, sinusoidal potential of 10mV, and frequency range of 100 kHz to 0.1 Hz. Using the Nernst equation, the experimental potential measured against (Ag/AgCl) was converted into the reversible hydrogen electrode potential (RHE).

3. Results and discussion

3.1. Crystal quality, morphology, and surface chemical composition characterizations

A powder XRD method was used to obtain XRD results for pristine Co_3O_4, CCR-0.1, CCR-0.2, and CCR-0.3. The recorded diffractograms are shown in Fig.1. At scanning angles of 30.99°, 36.51°, 38.20°, 44.40°, 55.13°, 58.79°, 64.60°, 73.37°, the diffraction patterns of pure Co_3O_4 correspond to crystal planes (220), (311), (222), (400), (422), (511) and (440), respectively. According to the XRD patterns, Co3O4 exhibits a cubic crystalline phase (JCPDS card no. 01-080-1544). The composite materials CCR-0.1, CCR-0.2, and CCR-0.3 have shown diffraction peaks at 2 theta angles of 38.56^o, 44.83^o, and 65.26^o, respectively, in the crystallographic planes (111), (200), and (220) of the nonstoichiometric phase of chromic $CrO_{0.87}$. These patterns confirm FTC card number 01-078-0722, which indicates cubic crystalline $CrO_{0.87}$ [53, 54]. From XRD analysis, it was noticed that the increasing concentration of $CrO_{0.87}$ in composite decreased the intensity of major peak (311) of Co_3O_4 as shown in Fig. 1. It was evident that Co_3O_4 reflections were observed in the hybrid material, indicating that Co_3O_4 and $CrO_{0.87}$ materials were incorporated in situ in a non-stoichiometric manner. According to the XRD analysis, the two theta angle has shifted significantly towards a lower angle, as shown in the figure to the right; Fig. 1. A large chromate ion in potassium chromate has produced a stress on crystal growth, resulting in a shift in the 2 theta angle. It is possible that this shift could lead to defects in the structure of the hybrid $CrO_{0.87}$ and Co_3O_4 material that may be exploited for lowering the overpotential of OERs. XRD measurements of the prepared materials revealed no other impurities. Additionally, we performed FTIR experiments on the prepared $CrO_{0.87}$ and Co_3O_4 hybrid materials to support the XRD results; Fig. S1. FTIR analysis of all the samples revealed similar inorganic peaks due to the presence of potassium bromide (KBr) used for making the pallets for each sample. [55-57]. However, there was only a significant difference observed between O-Co-O and Co-O metal oxide peaks at 667 cm^{-1} and 577 cm^{-1}, respectively [58, 59]. FTIR studies indicated that higher concentrations of potassium chromate resulted in a decrease in metal oxide peaks, which indicates in situ growth of $CrO_{0.87}$ and Co_3O_4.

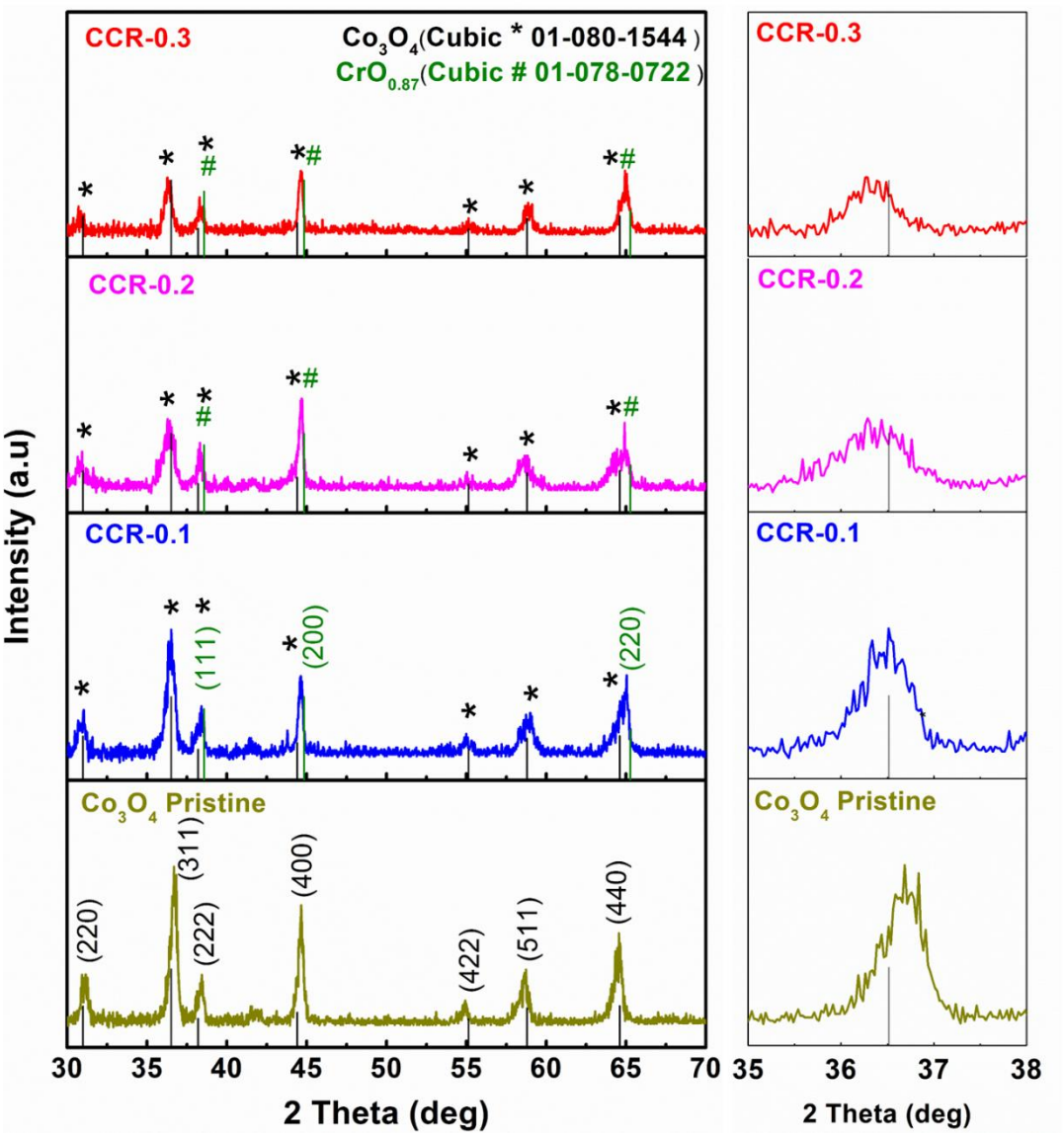

Fig. 1 X-ray diffractograms of pristine Co_3O_4, CCR-0.1, CCR-0.2 and CCR-0.3 and their relative shift in the two theta (right hand side).

SEM analysis indicates that pristine Co_3O_4, CCR-0.1, and CCR-0.2 exhibit similar needle-like structures composed of interconnected beads of approximately tens of nanometers in diameter (Figs. 2a-2c), whereas CCR-0.3 exhibits fewer ordered and smaller particles arranged in more or less spherical arrangements, Fig. 2d. In addition, the SEM analysis of CCR-0.3 after durability

test suggested that the morphological characteristics of hybrid $CrO_{0.87}$ into Co_3O_4 (CCR-0.3) are stable after long term performance.

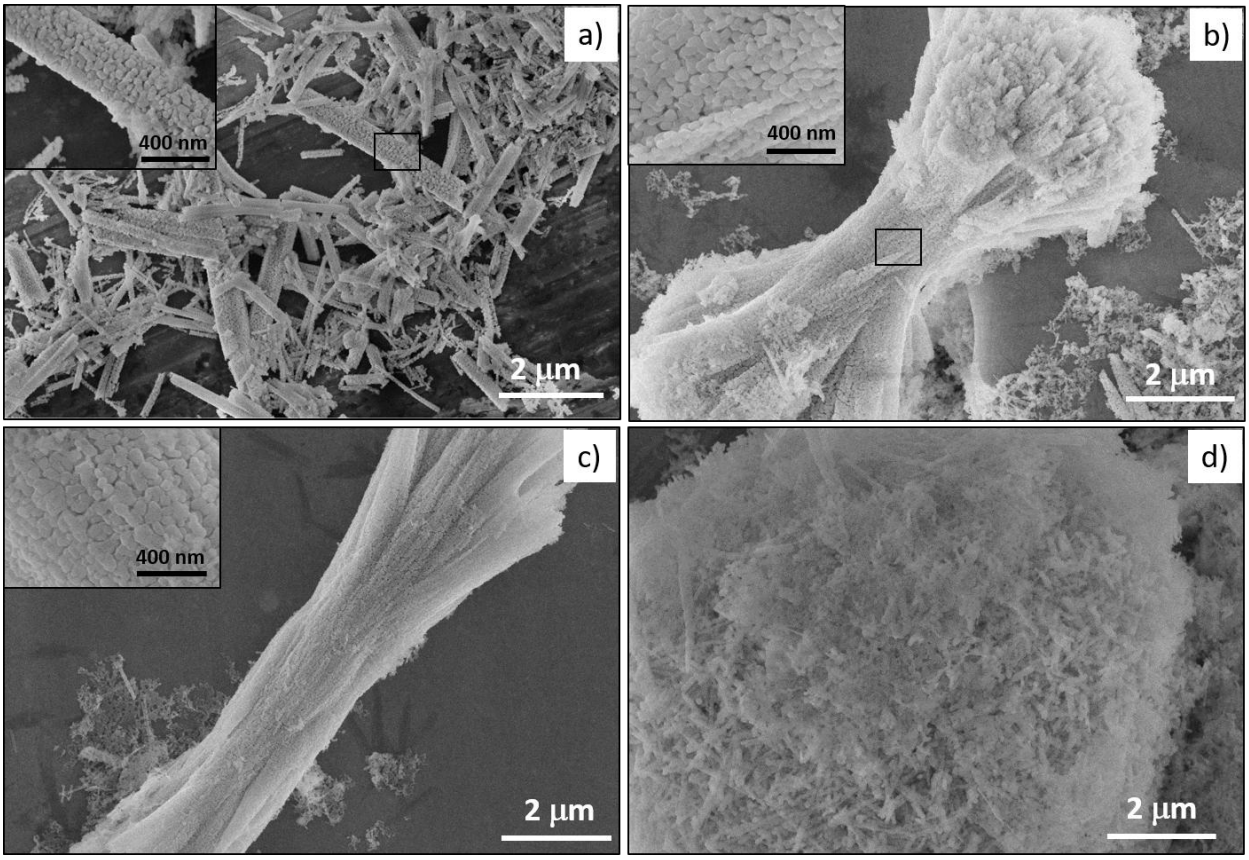

Fig. 2 SEM micrographs of **(a)** pristine Co_3O_4, **(b)** CCR-0.1, **(c)** CCR-0.2 and **(d)** CCR-0.3.

TEM micrographs of pristine Co_3O_4 at different magnifications are shown in Fig. 3(a-c). It is characteristic of a pure sample that the nanoparticles that comprise the microstructure are heterogeneous in size. Additionally, the morphology of the nanoparticles has changed from a spherical shape to a rectangle. The size distribution is quite heterogeneous, with smaller nanoparticles having a diameter of 30 nm and larger particles having a diameter of >100 nm.

TEM micrographs of CCR-0.3 at various magnifications are shown in Fig. 4(a-c). In the sample, there appears to be a large number of aggregates with a diameter of several microns. The induction of $CrO_{0.87}$ into Co_3O_4 shows a high degree of variation and irregular morphology, probably the result of many nanoparticles merging. The size distribution can therefore be

difficult to evaluate precisely for this reason. Further, some aggregates with a needle-like shape are dispersed in an irregular arrangement of the microaggregates.

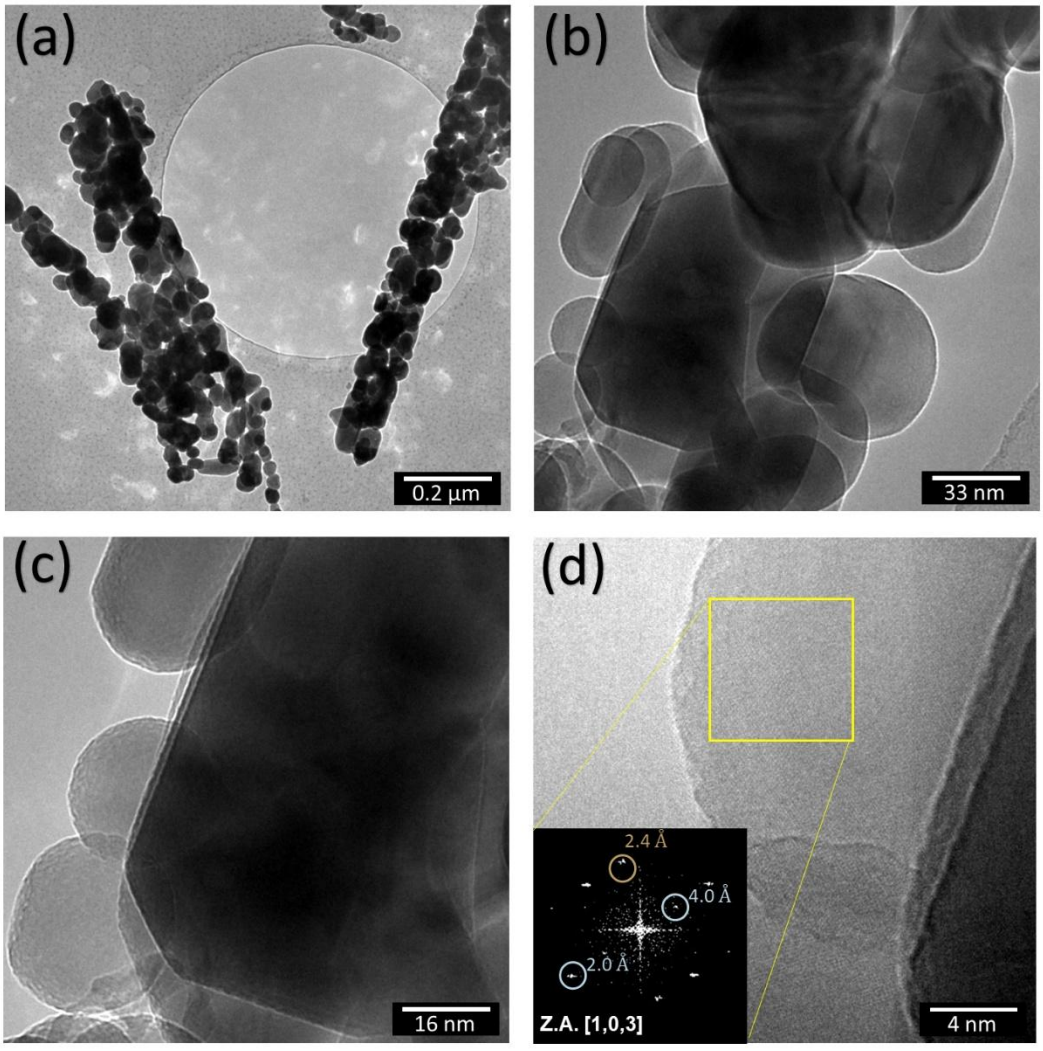

Fig. 3 (a-c) TEM micrographs of pristine Co_3O_4 at different magnifications **(d)** HR-TEM micrograph and FFT in the inset reporting the crystal pattern.

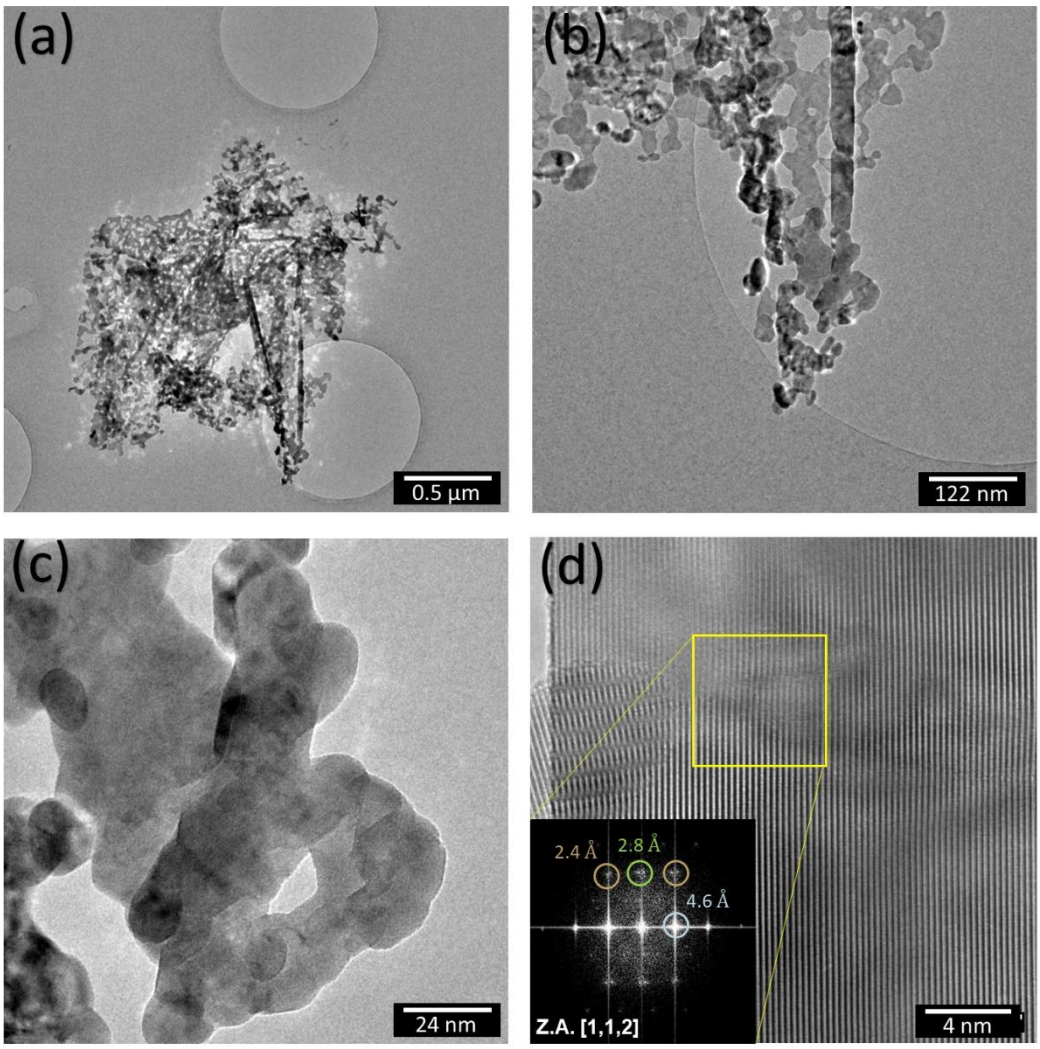

Fig. 4 (a-c) TEM micrographs of hybrid $CrO_{0.87}$ into Co_3O_4 (CCR-0.3) at different magnifications **(d)** HR-TEM micrograph and FFT in the inset reporting the crystal pattern.

Based on the HR-TEM image at high magnification, pristine Co_3O_4 is confirmed to have a crystalline structure as shown in Fig. 3(d). The crystal lattice of the particle is similar to that of Co_3O_4 with a spinel-like structure. Specifically, the crystal lattice does not differ when moving from a smaller to a larger nanoparticle, proving the same composition in both cases.

HR-TEM, however, has also validated the crystallinity of the CCR-0.3 material as shown in Fig. 4(d). This crystal structure resembles that of Co_3O_4, which has a spinel-like structure. In particular, the sample's surface is quite regular with large crystals. In most cases, the addition of $CrO_{0.87}$ to the preparation step does not affect the crystalline phase, but rather the morphology.

Micrographs of Co_3O_4 were taken using HAADF and STEM techniques at various magnifications as shown in Fig. S3. According to these images, both the morphology and the distribution of dimensions are in agreement with what was observed on TEM micrographs. While HAADF – STEM micrographs of CCR-0.3 confirmed what was observed in the TEM micrographs, making more visible the more condensed crystalline phase with respect to the pristine Co_3O_4 as seen in Fig. S4. Fig. S5 shows the position analysis of the pristine sample by EDS. The atomic percentage ratio between O and Co in the highlighted area (orange circle) is exactly what was expected with a value of 1.3. Furthermore, considering other specific points, the ratio does not change, indicating homogeneity in the composition. EDS mapping of the sample Cr doped is demonstrating that the Co content of the nanostructure is perfectly comparable with the signals of O and Cr, with their distributions having a similar morphology to those observed by STEM-HAADF micrographs, indicating a homogeneous composition; Fig. S6. Despite the increase in the O signal, probably caused by the presence of Cr in the form of oxide, the atomic percentages of the different chemical components do not permit confirmation of the crystal phase analysis. The atomic ratio of O to Co is 2.8 on average (normally, this ratio is 1.33 for Co_3O_4). Taking into account the different points on the EDS map, the ratio of Cr/Co is approximately 0.27 on average.

As with other transition metals, it is not straightforward to interpret Co 2p spectra, due to peak asymmetries, shake-up and loss structures, multiplet splitting, and, in this case, charging effects. Based on literature reports [60-62], a qualitative approach was adopted in order to minimize the uncertainty in peak assignment. As shown in Fig. 5A-B, the spectra of cobalt oxide powders were measured. In the spectrum, there are two prominent peaks, one located at about 780 eV (Co2p3/2), and the other at about 796 eV (Co2p1/2). In the high binding energy region of the major peak, a weak satellite structure is observed, which is commonly used to identify Co_3O_4 spinel structures [63, 64]. Fig. 5c shows that Cr $2p_{3/2}$ and Cr $2p_{1/2}$ deconvolved into CrO_2 as indicated by the peak in binding energy at 576.0 (585.7) eV.[65, 66]. The comparison between

the two samples, based on the overall lineshape observation, indicates a similar surface chemical composition for the two samples.

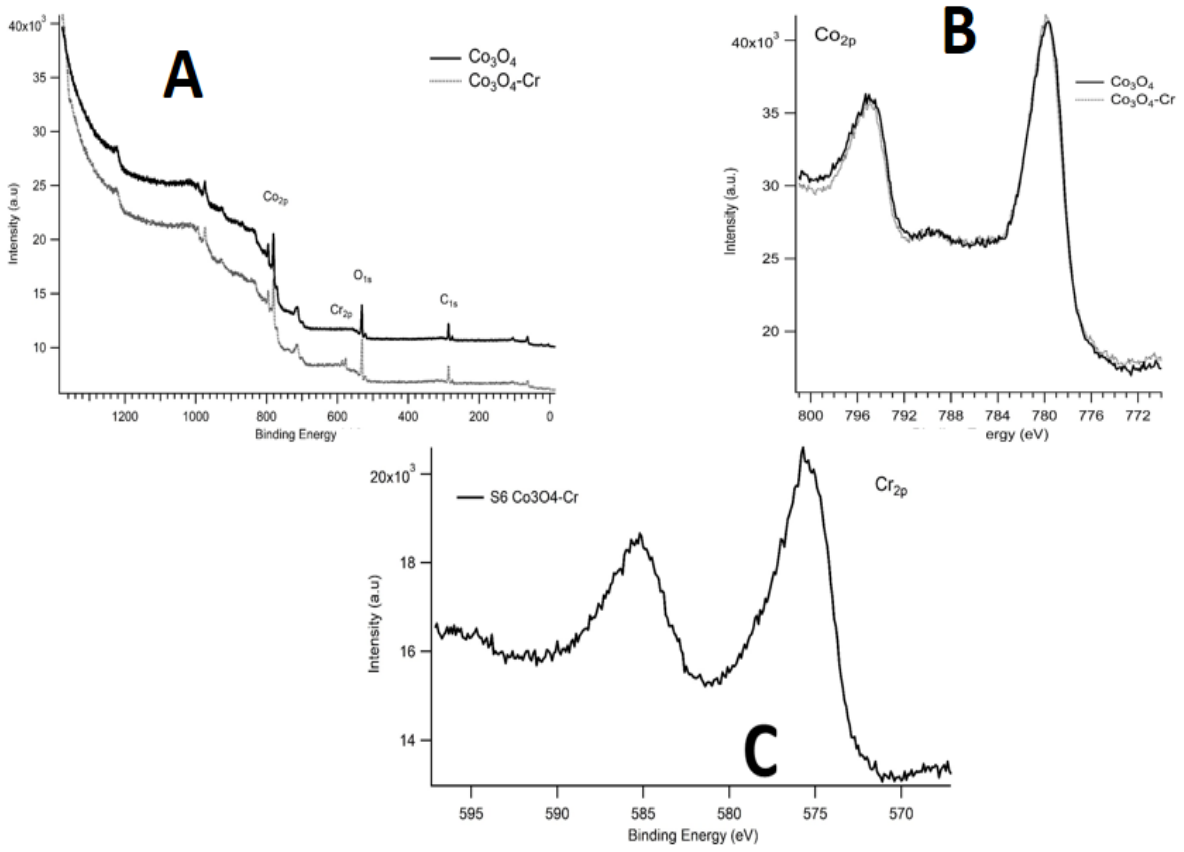

Fig. 5. (A) XPS survey scans for pure Co_3O_4 powder (solid line) and Cr-doped sample (dotted line). Photoemission peaks, reported toward binding energy, are labelled: Co2p and Cr2p structures are visible, together with C1s and O1s partially due to surface contamination, (B) Comparison of XPS Co2p spectra reported towards binding energy of pure Co_3O_4 (solid line) and the Cr doped Co_3O_4 (dotted line), (C)

3.2. Half Cell reaction

Electrochemical analysis was performed using linear sweep voltammetry (LSV) in 1.0 M KOH to determine the OER activities of $CrO_{0.87}$ as prepared into Co_3O_4 hybrid materials. Fig. 6a illustrates the LSV polarization curves of pristine Co_3O_4 and composites CCR-0.1, CCR-0.2, and CCR-0.3. The plot illustrates the onset potential information, which indicates that the highest onset potential was determined for the pure Co_3O_4 electrocatalyst of 1.569 Volts versus RHE,

while composite electrocatalysts, such as CCR-0.1, CCR-0.2 and CCR-0.3, had onset potentials of 1.49 Volts, 1.47 Volts and 1.45 Volts versus RHE, respectively. Further, Fig. 6(b) displays the overpotential histogram for different electrocatalysts derived from LSV curves, with a theoretical potential of 1.23 V vs RHE at a current density of 20 mA/cm^2. As compared to pristine Co_3O_4 (410 mV), CCR-0.1 (310 mV) and CCR-0.2 (270 mV), CCR-0.3 had the lowest overpotential of 255 mV. According to these results, $CrO_{0.87}$ impurities added to Co_3O_4 nanostructures lead to the formation of vacancies in the nanostructure. Therefore, a reduction in the overpotential of the electrocatalyst and significant catalytic activity have been observed. However, it was observed during experimental results (Fig. S7) that the addition of $CrO_{0.87}$ impurities in high concentration such as CCR-0.4 leads to deterioration of its reaction kinetics and decrease its OER performance. In Table S1, the CCR-0.3 catalyst outperforms other electrocatalysts reported. In terms of Tafel value and overpotential, CCR-0.3 demonstrated superior or equal performance to numerous recently reported electrocatalysts. These improvements in the activity of CCR-0.3 hybrid material could be explained by surface vacancies, abundant metallic chemical states, surface alteration, and tunable morphology as described by XRD, SEM, HRTEM, and XPS investigations.

The Tafel plot values were calculated from the linear region of the LSV curves and they provided information about OER kinetics. Pristine Co_3O_4, CCR-0.1, CCR-0.2, and CCR-0.3 have been determined to have Tafel values of 97 mV/dec, 72 mV/dec, 64 mV/dec, and 56 mV/dec, respectively as shown in Fig. (6c). Among the lowest Tafel values of CCR-0.3 (56 mV/dec), 56 mV/dec is representative of OER kinetics and serves as a confirmation of the possibility of swift OER reactions on the surface of the CCR-0.3 hybrid material. , Having a Tafel value that is similar to that of a noble metal catalyst (RuO_2), the newly designed in situ nonstoichiometric CCR-0.3 is likely to achieve practical and promising performance [67-69]. A generalized four-step process is followed by the transfer of four electrons in the OER process as described below.

Mechanism	**Step No.**
$M + OH^- \rightarrow MOH + e^-$	01.

$MOH + OH^- \rightarrow MO^- + H_2O$	02.
$MO^- \rightarrow MO + e^-$	03.
$MO \rightarrow 2M + O_2 + 2e^-$	04.

The theoretical Tafel values of OER kinetic steps were 120 mV/dec (step.1), 60 mV/dec (step.2), 40 mV/dec (step.3), and 15 mV/dec (step.4). [70]. An electrocatalyst prepared in this case yielded a Tafel value of 56 mV/dec, indicating that step 2 is the rate-limiting step. From the reaction kinetic of OER mechanism, it is suggested that the MOH + OH^->MO^-+H_2O is responsible reaction taking place due to doping of $CrO_{0.8}$ into Co_3O_4 nanostructured matrix that facilitates the oxygen vacancies to promote the reaction kinetics of OER activity.

In order to determine the double layer capacitance (Cdl) and electrochemical active surface area (ECSA) of the electrocatalysts, cyclic voltammetry (CV) was used. Fig. S10 shows the CV curves for various prepared samples analyzed at various scan rates including 30 mV/sec, 50 mV/sec, 70 mV/sec, 90 mV/sec, 110 mV/sec, and 130 mV/sec in the non-faradic region. The Cdl values were derived from CV data by plotting the linear fit slope of current densities at different scan rates as depicted in Fig. 6(d). Pristine Co_3O_4 exhibited the lowest capacitance value of 3.7 $mF.cm^{-2}$, while CCR-0.1, CCR-0.2 and CCR-0.3 showed ascending capacitance values of 17.1 $mF.cm^{-2}$, 13.8 $mF.cm^{-2}$ and 20.6 $mF.cm^{-2}$, respectively.

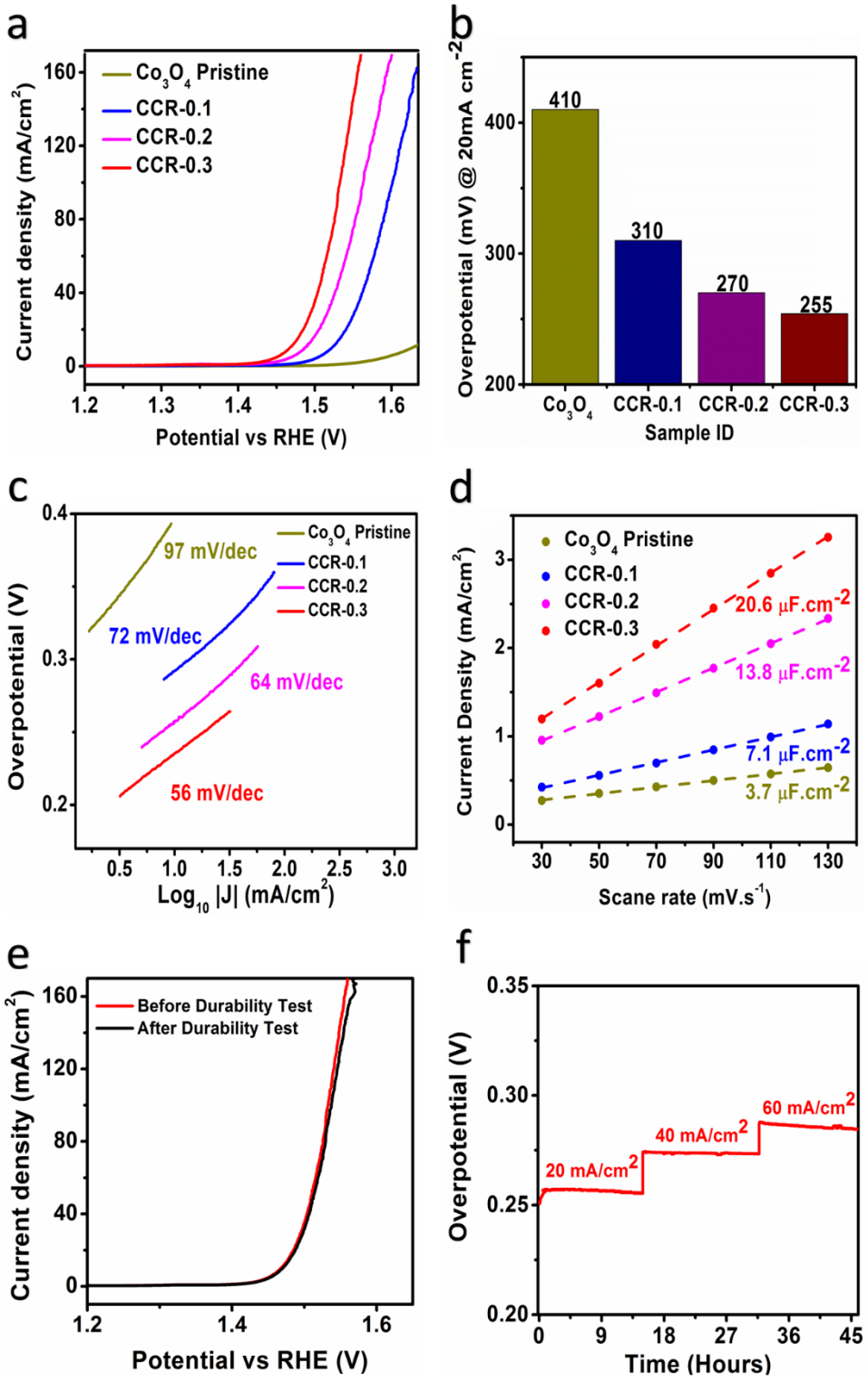

Fig.6 Electrochemical analysis (a) LSV curves of various electrocatalyst (b) Overpotential histogram (c) Tafel values plot (d) Double layer capacitance C_{dl} values plot (e) Stability curve of CCR-0.3 and (f) Chrono-potentiometric durability of CCR-0.3 at various current densities.

Moreover, the electrochemical active surface area of the catalysts prepared was also determined by determining their C_{dl} values. A summary of the computed ECSA values and the OER performance of each sample is shown in OER Table.1. As can be observed, the CCR-0.3 sample exhibits the highest active surface area of approximately 515 cm^2, making it an ideal candidate for advanced electrocatalytical applications.

To eliminate the effect of greater electrochemical surface area (ECSA) on OER performance, the LSV curves are normalized by ECSA[71]. Fig. S8 results show that CCR-0.3 exhibits significantly higher OER activity than CCR-0.2, CCR-0.1 and pristine Co_3O_4 samples, demonstrating that the improved OER activity is due to both an increased ECSA and the catalyst's improved intrinsic activity as a result of its optimized electronic structure. By contrasting the actual performance of catalysts, per-site turnover frequency (TOF) is used to better explain the intrinsic process for the improvement of OER activity. While computing the TOF, it is assumed that all metal atoms are active sites [72, 73]. The TOF value of corresponding catalyst can be seen in Fig. S9, was determined at 255 mV overpotential. As can be seen, the CCR-0.3 catalyst has exhibited significantly higher current density and TOF values (0.000909 $mA.cm^{-1}$, $0.37x10^{-2}$ s^{-1}) than CCR-0.2 (0.000620 $mA.cm^{-1}$, $0.25x10^{-2}$ s^{-1}) and pristine Co_3O_4 (0.000075 $mA.cm^{-1}$, $0.03x10^{-2}$ s^{-1}) suggesting that the $CrO_{0.8}$ dopants significantly influence the coordination environment and symmetry of Co sites, thereby significantly improving the intrinsic activity of active Co sites. Previous research often shown that this heteroatom doping approach greatly boosted TOF values [74, 75].

The stability test was conducted by measuring the LSV before and after the durability test. The stability of the CCR-0.3 catalyst is illustrated in Fig.6(e), and the polarization curve was almost the same as it was before, but a slight change was observed at the end of the curve due to small degradation of the catalyst. Nevertheless, the durability of CCR-0.3 electrocatalyst was tested by chronopotentiometric technique at different current densities (20 mA/cm^2, 40 mA/cm^2, 60 mA/cm^2) for 45 hours. It is evident from Fig. 6(f) that the potential of the catalyst did not decrease over a 45-hour period, and the variation in current densities did not affect its performance. It follows that the proposed electrocatalyst is capable of maintaining its functionality over an extended period of time.

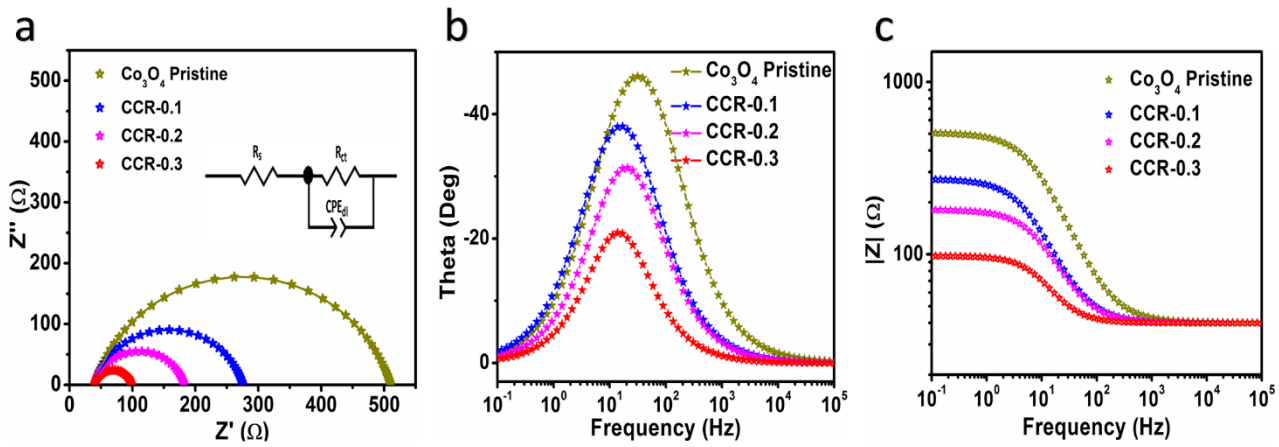

Fig.7 Electrochemical impedance spectroscopic analysis of Co_3O_4 pristine, CCR-0.1, CCR-0.2 and CCR-0.3 (a) Nyquist (b) Bode-1 and (c) Bode-2 plot.

In order to determine the charge transfer resistance (Rct) between electrode and electrolyte, electrochemical impedance spectroscopy (EIS) was performed. Data were analyzed using Z view software using equivalent circuits as described in Fig. 7(a) based on the results of the EIS test in 1.0 M KOH solution. According to the Nyquist plot of the prepared electrocatalyst shown in Fig. 7(a), all samples have similar solution resistances (R_S) since the test was conducted at a similar electrolyte concentration, i.e., 1.0M KOH. Furthermore, pristine Co_3O_4 has a higher estimated value of R_{ct} of 470 and the most effective catalyst (CCR-0.3) has a lower estimate of Rct of 58.2. Data from the EIS were used to calculate double layer capacitance values (CPE_{dl}) that are mentioned in the summarized features Table.1. It can be observed that the CCR-0.3 catalyst has the highest CPE_{dl} value. Based on these data, $CrO_{0.87}$ is effective against Co_3O_4 nanostructure that facilitates the movement of charges at the interface between electrode and electrolyte. Fig. 7 (b and c) illustrates bode plots 1 and 2. Bode plot-1 gives information about the catalyst's gain at a frequency level ranging from 10^6 Hz to 10^{-1} Hz. There are orderly gain features of 46.15°, 38.13°, 31.46° and 21.11° in pristine Co_3O_4, CCR-0.1, CCR-0.2 and CCR-0.3. In particular, the CCR-0.3 electrocatalyst outperforms the other three catalysts in terms of gain characteristics. However, CCR-0.3 ($CrO_{0.8}$@Co_3O_4) showed a lower maximum oscillation frequency than other electrocatalysts in the bode plot-2. Consequently, a longer electron recombination lifetime was achieved, which may have contributed to a higher adsorption of active species at the catalyst

interface. Therefore, $CrO_{0.8}$@ Co_3O_4 electrocatalyst is the most promising candidate for practical OER applications.

Table 1: Summarized OER features of presented catalysts.

Catalyst	Calculated from LSV	Calculated from EIS		Calculated from CV	
	Tafel Slope	**Charge Transfer Resistance**	**Double Layer Capacitance**	**Double Layer Capacitance**	**Electrochemically active surface area**
	B	R_{ct}	CPE_{dl}	C_{dl}	***ECSA***
	mV/dec	**Ω**	***mF***	mF/cm^2	cm^2
Co_3O_4 Pristine	97	470	0.049	3.7	92.5
CCR-0.1	72	235	0.15	7.1	177.5
CCR-0.2	64	142	0.23	13.8	345
CCR-0.3	56	58.2	0.32	20.6	515

4. Conclusions

The synthesis of ($CrO_{0.8}$@Co_3O_4) nano-electrocatalyst was carried out by co-precipitation. The (CCR-0.3) electrocatalyst was found to be an optimized electrocatalyst. XRD results confirmed the existence of a cubic phase of $CrO_{0.8}$ and Co_3O_4. Based on electrochemical investigations, CCR-0.3 exhibits the highest OER activity due to its low overpotential (255mV), near Tafel values (56 mV/dec) to bobel catalyst, and higher double layer capacitance values (20.6 $\mu F.cm^{-2}$) among all prepared electrocatalysts. Moreover, the electrocatalyst proposed was stable at a variety of current densities and durable for more than 45 hours, which makes it suitable for industrial applications. Additionally, this catalyst has a low charge transport resistance (58.2) and a high electrochemical active surface area (515 cm^2), which makes it easier to facilitate the movement of charge carriers at the interface. Based on these accumulated data, it can be concluded that the addition of $CrO_{0.8}$ to Co_3O_4 enhances its catalytic properties by modifying its morphological attributes, which is useful for a variety of applications.

Acknowledgments

We also extend our sincere appreciation to the Researchers Supporting Project Number (RSP2023R79) at King Saud University, Riyadh, Saudi Arabia. B. V. thank the platform “Microscopies, Microprobes and Metallography (3 M)” (Institut Jean Lamour, IJL, Nancy, France) for access to SEM facilities and F. Alnjiman for his valuable help. We also acknowledge partial funding of the Ajman University, Grant ID: DGSR ref. 2022-IRG-HBS-5

Conflict of Interest

Authors declare no competing interests in the resented research work

5. References

[1] Wang M, Wang G, Sun Z, Zhang Y, Xu D. Review of renewable energy-based hydrogen production processes for sustainable energy innovation. Global Energy Interconnection. 2019;2:436-43.

[2] Tao M, Azzolini JA, Stechel EB, Ayers KE, Valdez TI. Review—Engineering Challenges in Green Hydrogen Production Systems. Journal of The Electrochemical Society. 2022;169:054503.

[3] Agaton CB, Batac KIT, Reyes Jr EM. Prospects and challenges for green hydrogen production and utilization in the Philippines. International Journal of Hydrogen Energy. 2022;47:17859-70.

[4] Saqib N. Green energy, non-renewable energy, financial development and economic growth with carbon footprint: heterogeneous panel evidence from cross-country. Economic Research-Ekonomska Istraživanja. 2022:1-20.

[5] Ishaq H, Dincer I. A comparative evaluation of OTEC, solar and wind energy based systems for clean hydrogen production. Journal of Cleaner Production. 2020;246:118736.

[6] Dogaru L. The Main Goals of the Fourth Industrial Revolution. Renewable Energy Perspectives. Procedia Manufacturing. 2020;46:397-401.

[7] Zhang K, Zhou B, Or SW, Li C, Chung CY, Voropai N. Optimal Coordinated Control of Multi-Renewable-to-Hydrogen Production System for Hydrogen Fueling Stations. IEEE Transactions on Industry Applications. 2022;58:2728-39.

[8] Pajak M, Brus G, Szmyd JS. Catalyst Distribution Optimization Scheme for Effective Green Hydrogen Production from Biogas Reforming. Energies. 2021;14:5558.

[9] Caglayan DG, Heinrichs HU, Robinius M, Stolten D. Robust design of a future 100% renewable european energy supply system with hydrogen infrastructure. International Journal of Hydrogen Energy. 2021;46:29376-90.

[10] Zhiznin SZ, Vassilev S, Gusev AL. Economics of secondary renewable energy sources with hydrogen generation. International Journal of Hydrogen Energy. 2019;44:11385-93.

[11] Schönauer A-L, Glanz S. Hydrogen in future energy systems: Social acceptance of the technology and its large-scale infrastructure. International Journal of Hydrogen Energy. 2022;47:12251-63.

[12] Kumbhar VS. Recent advances in water-splitting electrocatalysts based on manganese oxide. 2019:14.

[13] Liu PF, Yin H, Fu HQ, Zu MY, Yang HG, Zhao H. Activation strategies of water-splitting electrocatalysts. Journal of Materials Chemistry A. 2020;8:10096-129.

[14] Tahira A. Electrochemical water splitting based on metal oxide composite nanostructures. Linköping: Linköping University Electronic Press; 2020.

[15] Wang S, Lu A, Zhong CJ. Hydrogen production from water electrolysis: role of catalysts. Nano Converg. 2021;8:4.

[16] Hanan A, Shu D, Aftab U, Cao D, Laghari AJ, Solangi MY, et al. Co2FeO4@rGO composite: Towards trifunctional water splitting in alkaline media. International Journal of Hydrogen Energy. 2022;47:33919-37.

[17] Li Y, Chen J, Cai P, Wen Z. An electrochemically neutralized energy-assisted low-cost acid-alkaline electrolyzer for energy-saving electrolysis hydrogen generation. Journal of Materials Chemistry A. 2018;6:4948-54.

[18] Suen N-T, Hung S-F, Quan Q, Zhang N, Xu Y-J, Chen HM. Electrocatalysis for the oxygen evolution reaction: recent development and future perspectives. Chemical Society Reviews. 2017;46:337-65.

[19] Jiang A, Nidamanuri N, Zhang C, Li Z. Ionic-Liquid-Assisted One-Step Synthesis of CoO Nanosheets as Electrocatalysts for Oxygen Evolution Reaction. ACS Omega. 2018;3:10092-8.

[20] Yuan N, Jiang Q, Li J, Tang J. A review on non-noble metal based electrocatalysis for the oxygen evolution reaction. Arabian Journal of Chemistry. 2020;13:4294-309.
[21] Younis MA, Lyu S, Zhao Q, Lei C, Zhang P, Yang B, et al. Noble metal-free two dimensional carbon-based electrocatalysts for water splitting. BMC Materials. 2019;1:6.
[22] Abdul Hanan MYS, Aqeel Ahmed Shah, Umair Aftab, Zahoor Ahmed Ibupoto, Muhammad Ishaque Abro, Muhammad Nazim Lakhan, Irfan Ali Soomro, Elmuez A Dawi, Elfatih Mustafa, Brigitte Vigolo, Aneela Tahira, Zafar Hussain Ibupoto. PdO@ CoSe 2 composites: efficient electrocatalysts for water oxidation in alkaline media. RSC Advances. 2023;13:743-55.
[23] Guo B-Y, Zhang X-Y, Ma X, Chen T-S, Chen Y, Wen M-L, et al. RuO2/Co3O4 Nanocubes based on Ru ions impregnation into prussian blue precursor for oxygen evolution. International Journal of Hydrogen Energy. 2020;45:9575-82.
[24] Liu H, Xia G, Zhang R, Jiang P, Chen J, Chen Q. MOF-derived RuO2/Co3O4 heterojunctions as highly efficient bifunctional electrocatalysts for HER and OER in alkaline solutions. RSC Advances. 2017;7:3686-94.
[25] Reier T, Oezaslan M, Strasser P. Electrocatalytic Oxygen Evolution Reaction (OER) on Ru, Ir, and Pt Catalysts: A Comparative Study of Nanoparticles and Bulk Materials. ACS Catalysis. 2012;2:1765-72.
[26] Song F, Bai L, Moysiadou A, Lee S, Hu C, Liardet L, et al. Transition Metal Oxides as Electrocatalysts for the Oxygen Evolution Reaction in Alkaline Solutions: An Application-Inspired Renaissance. Journal of the American Chemical Society. 2018;140:7748-59.
[27] Goswami C, Hazarika KK, Bharali P. Transition metal oxide nanocatalysts for oxygen reduction reaction. Materials Science for Energy Technologies. 2018;1:117-28.
[28] Song K, Feng Y, Zhang W, Zheng W. MOFs fertilized transition-metallic single-atom electrocatalysts for highly-efficient oxygen reduction: Spreading the synthesis strategies and advanced identification. Journal of Energy Chemistry. 2022;67:391-422.
[29] Wang J, Yue X, Yang Y, Sirisomboonchai S, Wang P, Ma X, et al. Earth-abundant transition-metal-based bifunctional catalysts for overall electrochemical water splitting: A review. Journal of Alloys and Compounds. 2020;819:153346.
[30] Ibupoto ZH, Tahira A, Shah AA, Aftab U, Solangi MY, Leghari JA, et al. NiCo2O4 nanostructures loaded onto pencil graphite rod: An advanced composite material for oxygen evolution reaction. International Journal of Hydrogen Energy. 2022;47:6650-65.
[31] Tahira A, Aftab U, Solangi MY, Gradone A, Morandi V, Medany SS, et al. Facile deposition of palladium oxide (PdO) nanoparticles on CoNi2S4microstructures towards enhanced oxygen evolution reaction. Nanotechnology. 2022;33.
[32] Aftab U, Tahira A, Gradone A, Morandi V, Abro MI, Baloch MM, et al. Two step synthesis of TiO2–Co3O4 composite for efficient oxygen evolution reaction. International Journal of Hydrogen Energy. 2021;46:9110-22.
[33] Shuai C, Mo Z, Niu X, Yang X, Liu G, Wang J, et al. Hierarchical NiCo2S4 nanosheets grown on graphene to catalyze the oxygen evolution reaction. Journal of Materials Science. 2020;55:1627-36.
[34] Kaneti YV, Guo Y, Septiani NLW, Iqbal M, Jiang X, Takei T, et al. Self-templated fabrication of hierarchical hollow manganese-cobalt phosphide yolk-shell spheres for enhanced oxygen evolution reaction. Chemical Engineering Journal. 2021;405:126580.
[35] Song C, Liu Y, Wang Y, Tang S, Li W, Li Q, et al. Highly efficient oxygen evolution and stable water splitting by coupling NiFe LDH with metal phosphides. Science China Materials. 2021;64:1662-70.
[36] Li Z, Jiang Z, Zhu W, He C, Wang P, Wang X, et al. Facile preparation of CoSe2 nano-vesicle derived from ZIF-67 and their application for efficient water oxidation. Applied Surface Science. 2020;504:144368.

[37] Zhang J, Xu Q, Wang J, Hu Y, Jiang H, Li C. Heterointerface engineered NiFe(OH)x/Ni3S2 electrocatalysts to overcome the scaling relationship for ultrahigh-current-density water oxidation. Science China Materials. 2023;66:634-40.
[38] Hanan A, Solangi MY, Jaleel laghari A, Shah AA, Aftab U, Ibupoto ZA, et al. PdO@CoSe2 composites: efficient electrocatalysts for water oxidation in alkaline media. RSC Advances. 2023;13:743-55.
[39] Solangi MY, Aftab U, Tahira A, Abro MI, Mazarro R, Morandi V, et al. An efficient palladium oxide nanoparticles@Co3O4 nanocomposite with low chemisorbed species for enhanced oxygen evolution reaction. International Journal of Hydrogen Energy. 2021.
[40] Biesinger MC, Payne BP, Grosvenor AP, Lau LWM, Gerson AR, Smart RSC. Resolving surface chemical states in XPS analysis of first row transition metals, oxides and hydroxides: Cr, Mn, Fe, Co and Ni. Applied Surface Science. 2011;257:2717-30.
[41] Bai C, Wei S, Deng D, Lin X, Zheng M, Dong Q. A nitrogen-doped nano carbon dodecahedron with Co@Co3O4 implants as a bi-functional electrocatalyst for efficient overall water splitting. Journal of Materials Chemistry A. 2017;5:9533-6.
[42] Gong Y, Zhi Y, Lin Y, Zhou T, Li J, Jiao F, et al. Controlled synthesis of bifunctional particle-like Mo/Mn-NixSy/NF electrocatalyst for highly efficient overall water splitting. Dalton Transactions. 2019;48:6718-29.
[43] Wu Y, Xiao Z, Jin Z, Li X, Chen Y. The cobalt carbide/bimetallic CoFe phosphide dispersed on carbon nanospheres as advanced bifunctional electrocatalysts for the ORR, OER, and rechargeable Zn-air batteries. J Colloid Interface Sci. 2021;590:321-9.
[44] Mehboob A, Gilani SR, Anwar A, Sadiqa A, Akbar S, Patujo J. Nanoscale cobalt-oxide electrocatalyst for efficient oxygen evolution reactions in alkaline electrolyte. Journal of Applied Electrochemistry. 2021;51:691-702.
[45] Zhu M, Yu S, Ge R, Feng L, Yu Y, Li Y, et al. Cobalt Oxide Supported on Phosphorus-Doped g-C3N4 as an Efficient Electrocatalyst for Oxygen Evolution Reaction. ACS Applied Energy Materials. 2019;2:4718-29.
[46] Bhatti AL, Aftab U, Tahira A, Abro MI, Kashif samoon M, Aghem MH, et al. Facile doping of nickel into Co_3O_4 nanostructures to make them efficient for catalyzing the oxygen evolution reaction. RSC Advances. 2020;10:12962-9.
[47] Abdul Hanan Samo UA, Muhammad Yameen, Abdul Jaleel Laghari, Mukhtiar Ahmed, Muhammmad Nazim Lakhan, Altaf Hussain Shar, Ali Asif, Amir Ali. MAGNESIUM DOPED COBALT-OXIDE COMPOSITE FOR ACTIVE OXYGEN EVOLUTION REACTION. Journal of Applied and Emerging Sciences. 2021;11:210-6.
[48] Hanan A, Laghari AJ, Solangi MY, Aftab U, Abro MI, Cao D, et al. CdO/Co_3O_4 Nanocomposite as an Efficient Electrocatalyst for Oxygen Evolution Reaction in Alkaline Media. International Journal of Engineering Science Technologies. 2022;6:1-10.
[49] Bhatti AL, Aftab U, Tahira A, Abro MI, Mari RH, Samoon MK, et al. An Efficient and Functional Fe_3O_4/Co_3O_4 Composite for Oxygen Evolution Reaction. Journal of Nanoscience and Nanotechnology. 2021;21:2675-80.
[50] Laghari AJ, Aftab U, Tahira A, Shah AA, Gradone A, Solangi MY, et al. MgO as promoter for electrocatalytic activities of Co3O4–MgO composite via abundant oxygen vacancies and Co2+ ions towards oxygen evolution reaction. International Journal of Hydrogen Energy. 2022.
[51] Flores CLI, Balela MDL. Electrocatalytic oxygen evolution reaction of hierarchical micro/nanostructured mixed transition cobalt oxide in alkaline medium. Journal of Solid State Electrochemistry. 2020;24:891-904.
[52] Badruzzaman A, Yuda A, Ashok A, Kumar A. Recent advances in cobalt based heterogeneous catalysts for oxygen evolution reaction. Inorganica Chimica Acta. 2020;511:119854.
[53] Carneiro E, Parreira NMG, Vuchkov T, Cavaleiro A, Ferreira J, Andritschky M, et al. Cr-Based Sputtered Decorative Coatings for Automotive Industry. Materials (Basel, Switzerland). 2021;14.

[54] Gandhi AC, Li TY, Chan TS, Wu SY. Short-Range Correlated Magnetic Core-Shell CrO_2/Cr_2O_3 Nanorods: Experimental Observations and Theoretical Considerations. Nanomaterials (Basel, Switzerland). 2018;8.
[55] Galli M, Guerrini A, Cauteruccio S, Thakare P, Dova D, Orsini F, et al. Superparamagnetic iron oxide nanoparticles functionalized by peptide nucleic acids. RSC Advances. 2017;7:15500-12.
[56] Banerjee A SS, Banerjee R. Melanin from the Nitrogen-Fixing Bacterium Azotobacter chroococcum: A Spectroscopic Characterization. PLoS ONE. 2014;9:e84574.
[57] Kricheldorf HR, Chatti S, Schwarz G, Krüger R-P. Macrocycles 27: Cyclic aliphatic polyesters of isosorbide. Journal of Polymer Science Part A: Polymer Chemistry. 2003;41:3414-24.
[58] Laghari AJ, Aftab U, Shah AA, Solangi MY, Abro MI, Al-Saeedi SI, et al. Surface modification of Co3O4 nanostructures using wide range of natural compounds from rotten apple juice for the efficient oxygen evolution reaction. International Journal of Hydrogen Energy. 2023.
[59] Muhammad Yameen Solangi AHS, Abdul Jaleel Laghari, Umair Aftab, Muhammad Ishaque Abro, Muhammad Imran Irfan. MnO2@ Co3O4 nanocomposite based electrocatalyst for effective oxygen evolution reaction. Sukkur IBA Journal of Emerging Technologies. 2022;5:32-40.
[60] Xu Q, Zhang J, Zhang H, Zhang L, Chen L, Hu Y, et al. Atomic heterointerface engineering overcomes the activity limitation of electrocatalysts and promises highly-efficient alkaline water splitting. Energy & Environmental Science. 2021;14:5228-59.
[61] Zhang H, Zhang J, Li Y, Jiang H, Jiang H, Li C. Continuous oxygen vacancy engineering of the Co3O4 layer for an enhanced alkaline electrocatalytic hydrogen evolution reaction. Journal of Materials Chemistry A. 2019;7:13506-10.
[62] Zhang J, Xu Q, Wang J, Li Y, Jiang H, Li C. Dual-defective Co3O4 nanoarrays enrich target intermediates and promise high-efficient overall water splitting. Chemical Engineering Journal. 2021;424:130328.
[63] Gautier JL, Ríos E, Gracia M, Marco JF, Gancedo JR. Characterisation by X-ray photoelectron spectroscopy of thin MnxCo3−xO4(1≥x≥0) spinel films prepared by low-temperature spray pyrolysis. Thin Solid Films. 1997;311:51-7.
[64] G. A. Carson MHNaMAL. Epitaxial growth of Co3O4 on CoO(100). Journal of Vacuum Science & Technology A. 1996;14:1637-42.
[65] N.F. Heinig HJ, K.T. Leung. Fabrication of epitaxial CrO2 nanostructures directly on MgO (100) by pulsed laser deposition. Applied Physics Letters. 2007;91:253102.
[66] X. W. Li AG, Giang Xiao. Influence of strain on the magnetic properties of epitaxial (100) chromium dioxide (CrO2) films. Applied Physics Letters. 1999;75:713–5.
[67] Wasalathanthri RN, Jeffrey S, Awni RA, Sun K, Giolando DM. Electrodeposited Copper–Cobalt–Phosphide: A Stable Bifunctional Catalyst for Both Hydrogen and Oxygen Evolution Reactions. ACS Sustainable Chemistry & Engineering. 2019;7:3092-100.
[68] Lu XF, Chen Y, Wang S, Gao S, Lou XW. Interfacing Manganese Oxide and Cobalt in Porous Graphitic Carbon Polyhedrons Boosts Oxygen Electrocatalysis for Zn–Air Batteries. Advanced Materials. 2019;31:1902339.
[69] Cai Z, Bu X, Wang P, Su W, Wei R, Ho JC, et al. Simple and cost effective fabrication of 3D porous core–shell Ni nanochains@NiFe layered double hydroxide nanosheet bifunctional electrocatalysts for overall water splitting. Journal of Materials Chemistry A. 2019;7:21722-9.
[70] Aftab U, Tahira A, Mazzaro R, Abro MI, Baloch MM, Willander M, et al. The chemically reduced $CuO–Co_3O_4$ composite as a highly efficient electrocatalyst for oxygen evolution reaction in alkaline media. Catalysis Science & Technology. 2019;9:6274-84.
[71] Huang Y, Jiang L-W, Shi B-Y, Ryan KM, Wang J-J. Highly Efficient Oxygen Evolution Reaction Enabled by Phosphorus Doping of the Fe Electronic Structure in Iron–Nickel Selenide Nanosheets. Advanced Science. 2021;8:2101775.

[72] Anantharaj S, Karthik PE, Noda S. The Significance of Properly Reporting Turnover Frequency in Electrocatalysis Research. Angewandte Chemie International Edition. 2021;60:23051-67.
[73] Wu Z-P, Lu XF, Zang S-Q, Lou XW. Non-Noble-Metal-Based Electrocatalysts toward the Oxygen Evolution Reaction. Advanced Functional Materials. 2020;30:1910274.
[74] Xu J, Li J, Xiong D, Zhang B, Liu Y, Wu K-H, et al. Trends in activity for the oxygen evolution reaction on transition metal (M = Fe, Co, Ni) phosphide pre-catalysts. Chemical Science. 2018;9:3470-6.
[75] Zhang SL, Guan BY, Lu XF, Xi S, Du Y, Lou XW. Metal Atom-Doped Co3O4 Hierarchical Nanoplates for Electrocatalytic Oxygen Evolution. Advanced Materials. 2020;32:2002235.

Supporting Information

In-situ growth of nonstoichiometric $CrO_{0.87}$ and Co_3O_4 hybrid system for the enhanced electrocatalytic water splitting in alkaline media

Muhammad Yameen Solangi[a], Umair aftab[a], Aneela Tahira[c], Abdul Hanan[d], Monica Montecchi[f], Luca Pasquali[g.h.i], Matteo Tonezzer[L], Raffaello Mazzaro[e], Vittorio Morandi[e], Abdul Jaleel Laghari[a], Ayman Nafady[k], Muhammad Ishaq Abro[a], Melanie Emo[j], Brigitte Vigolo[j], Elmuez Dawi[m], Elfatih Mustafa[n], and Zafar Hussain Ibupoto[b].

[a]Department of Metallurgy and Materials Engineering, Mehran University of Engineering and Technology, 76080, Jamshoro, Pakistan.

[b]Dr M. A. Kazi Institute of Chemistry University of Sindh, Jamshoro, 76080, Pakistan.

[a]Institute of Chemistry, Shah Abdul Latif University Khairpur Mirs, Sindh, Pakistan.

[d]Key Laboratory of Superlight Material and Surface Technology, Ministry of Education, College of Materials Science and Chemical Engineering, Harbin Engineering University, 150001, Harbin, PR China.

[e]Department of science and technology, CNR IMM, Bologna, Italy.

[f]Engineering Department, University of Modena and Reggio Emilia, Modena, Italy.

[g]Engineering Department, University of Modena and Reggio Emilia, Modena, Italy.

[h]Chemistry, IOM-CNR Institute, Trieste, Italy.

[i]Department of Physics, University of Johannesburg, Auckland Park, South Africa.

[j]Université de Lorraine, CNRS, IJL, F-54000 Nancy, France.

[k]Department of Chemistry, College of Science, King Saud University, Riyadh 11451, Saudi Arabia.

[L]MEM-CNR, Sede di Trento-FBK, Trento, Italy.

[m]Nonlinear Dynamics Research Center (NDRC), Ajman University, Ajman, P.O. Box 346, United Arab Emirates.

[n]Department of Science and Technology (ITN), Linköping University, Campus Norrköping, 601 74, Norrköping, Sweden.

[*]**Corresponding author (s):** Zafar Hussain Ibupoto

E-mail: zaffar.ibhupoto@usindh.edu.pk

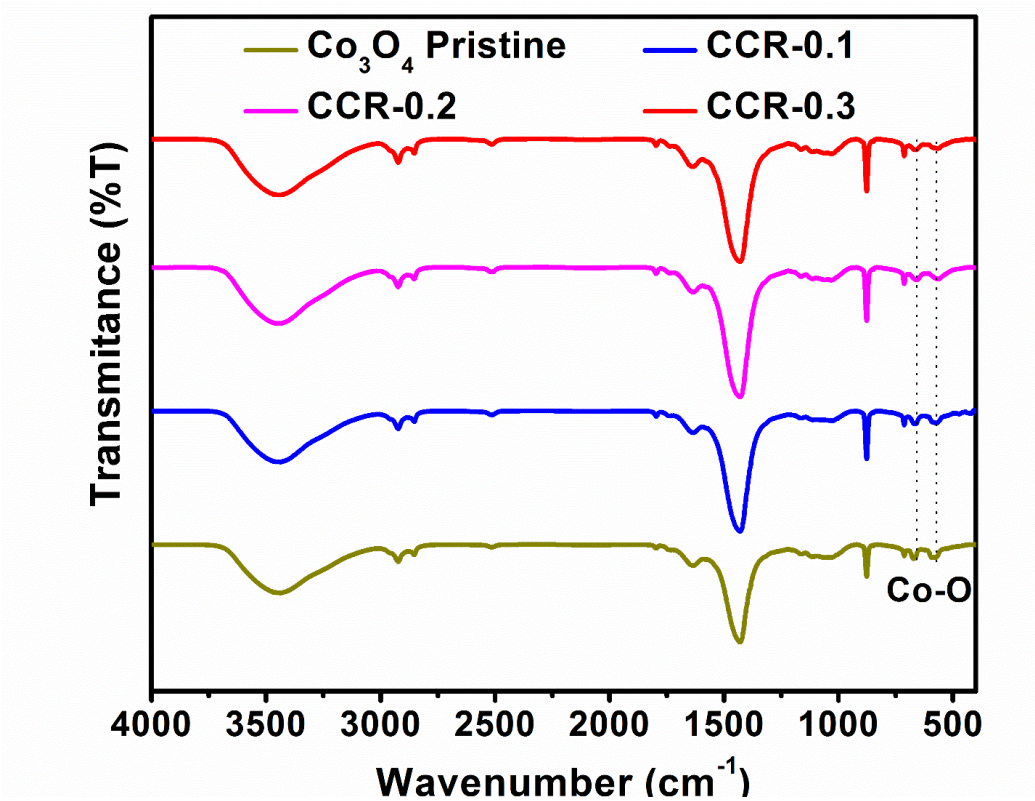

Fig. S1 Fourier Transform Infrared Spectroscopy of Co_3O_4 pristine, CCR-0.1, CCR-0.2 and CCR-0.3

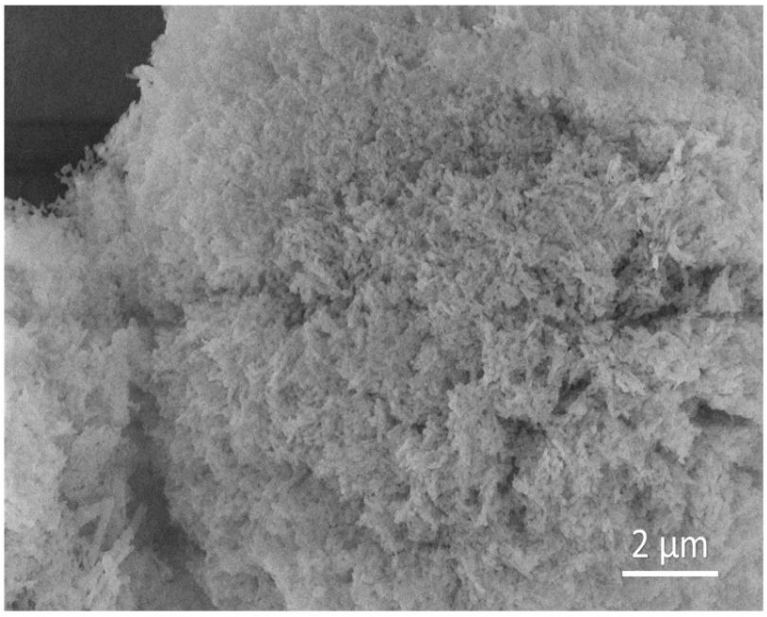

Fig. S2 SEM micrographs of hybrid $CrO_{0.87}$ into Co_3O_4 (CCR-0.3) after durability test.

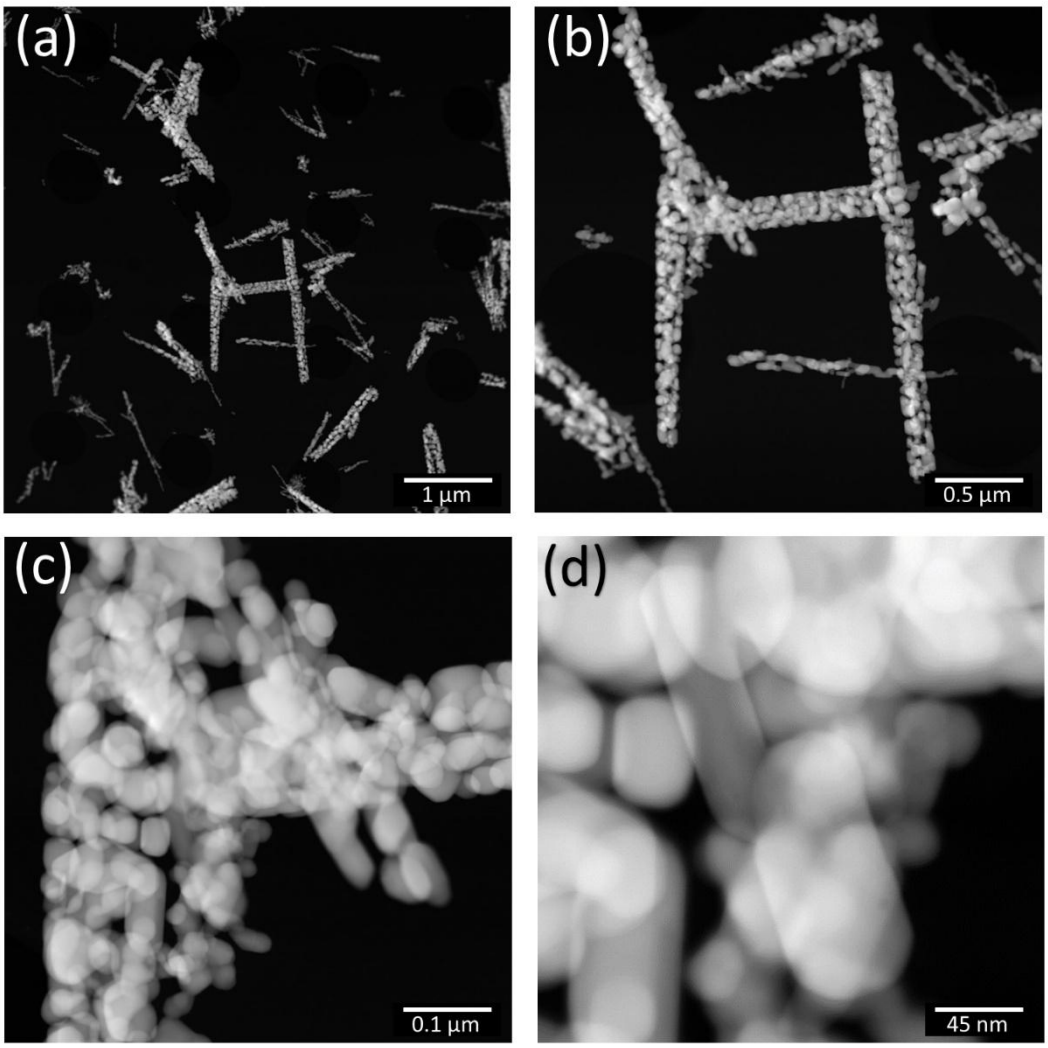

Fig. S3 HAADF – STEM micrographs of Co_3O_4 pristine at different magnifications.

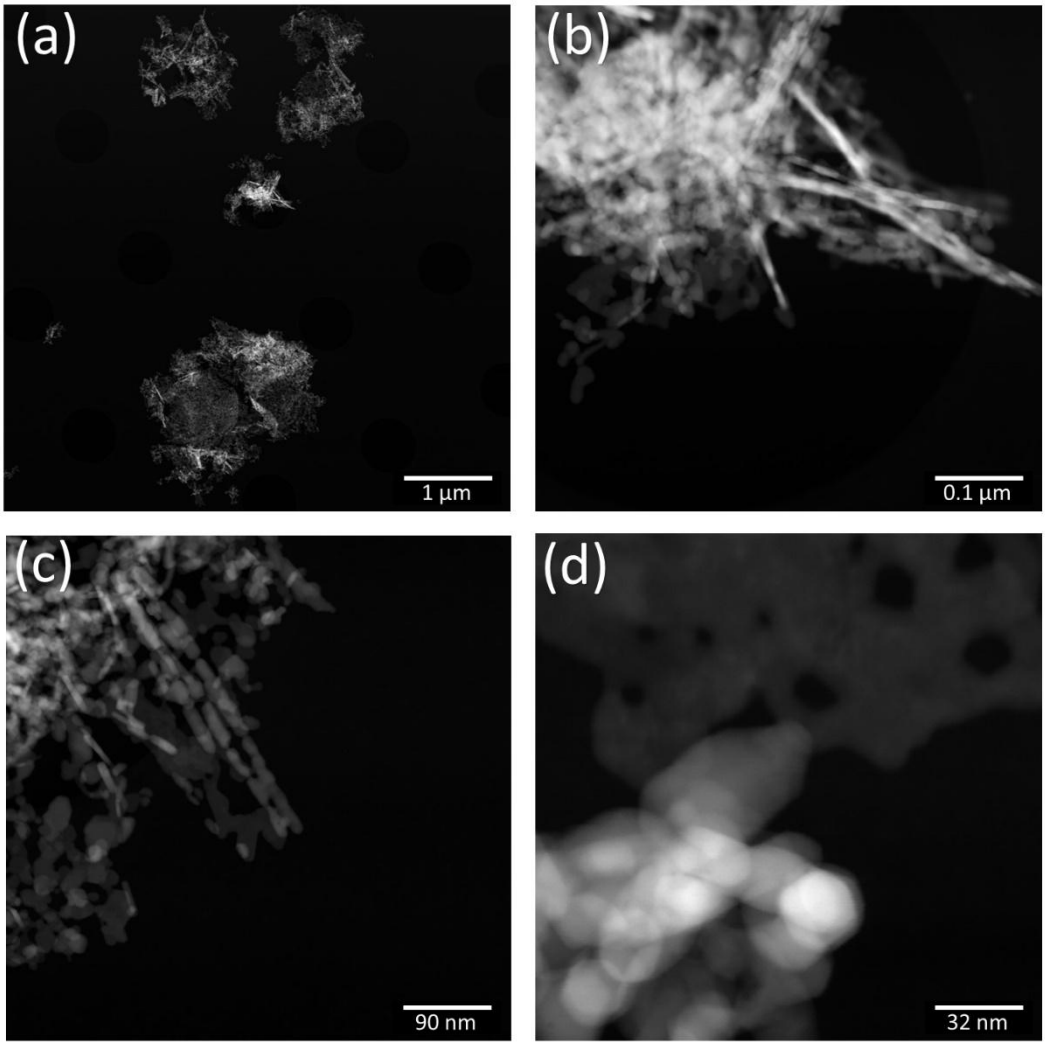

Fig. S4 HAADF – STEM micrographs of CCR-0.3 at different magnifications.

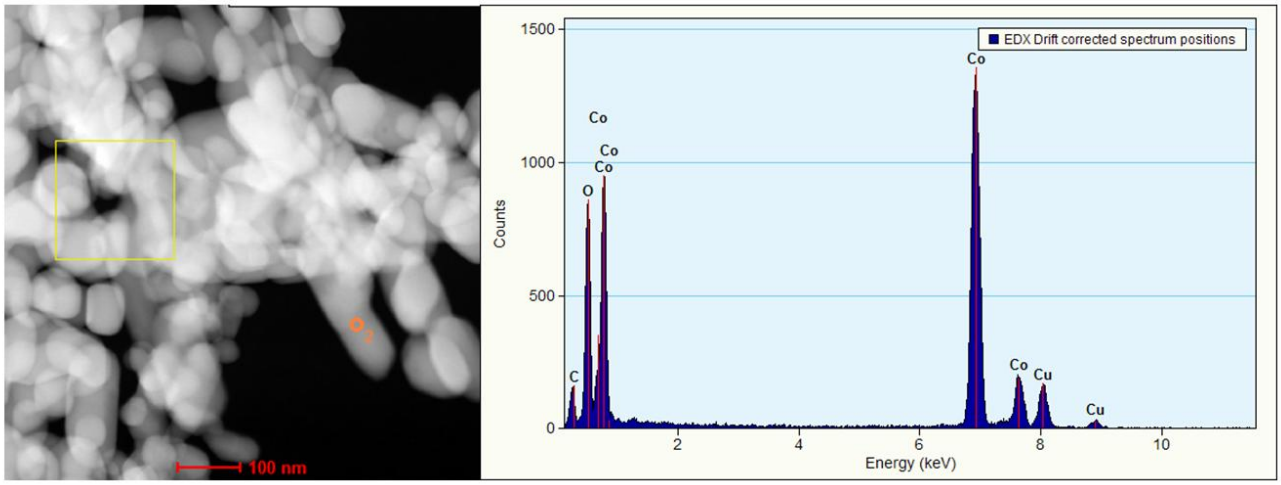

Fig. S5 STEM-EDS analysis of the pristine sample Co_3O_4.

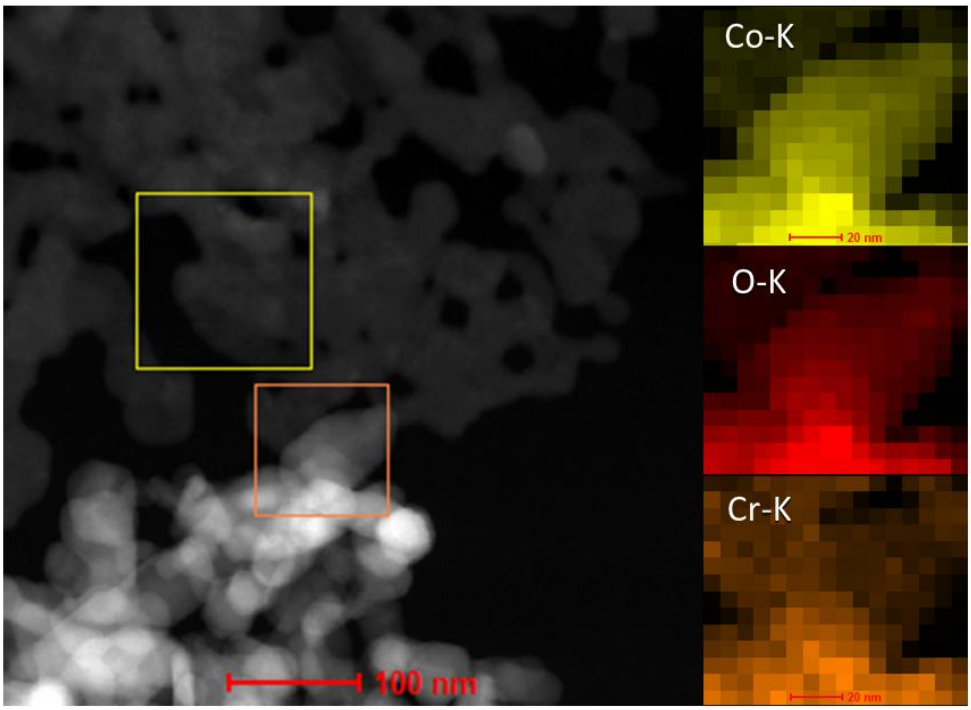

Fig. S6 STEM-EDS mapping of the CCR-0.3 displaying Cr as doping.

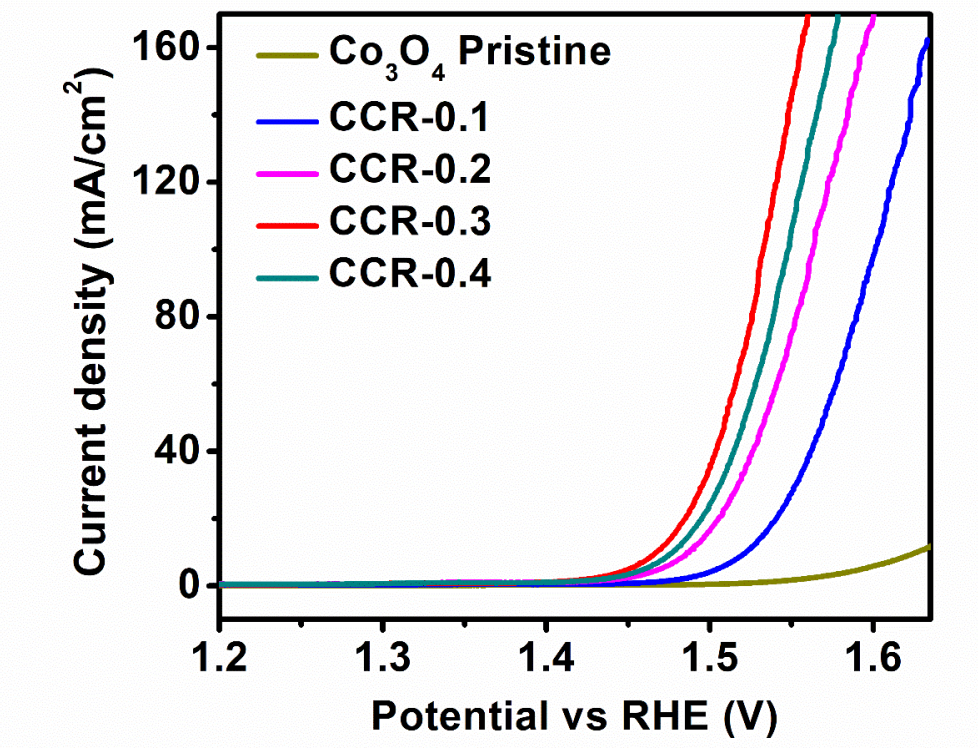

Fig. S7 LSV curves of various electrocatalyst along with high concentration (CCR-0.4).

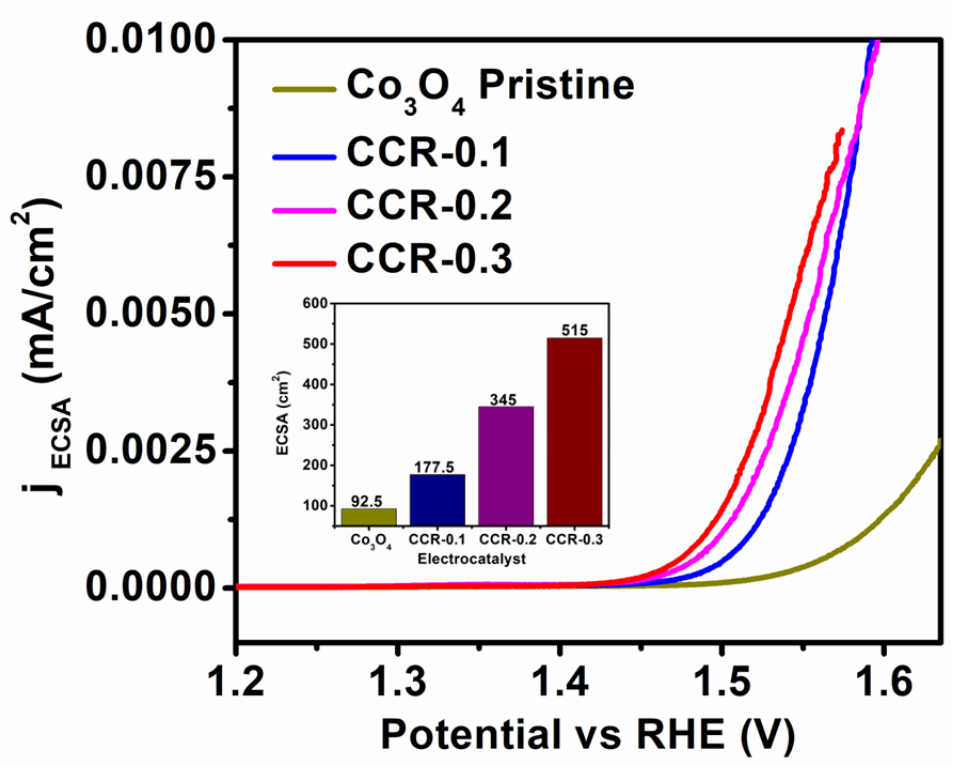

Fig. S8 ECSA-normalized LSV curves (Inset: a bar chart of the ECSA)

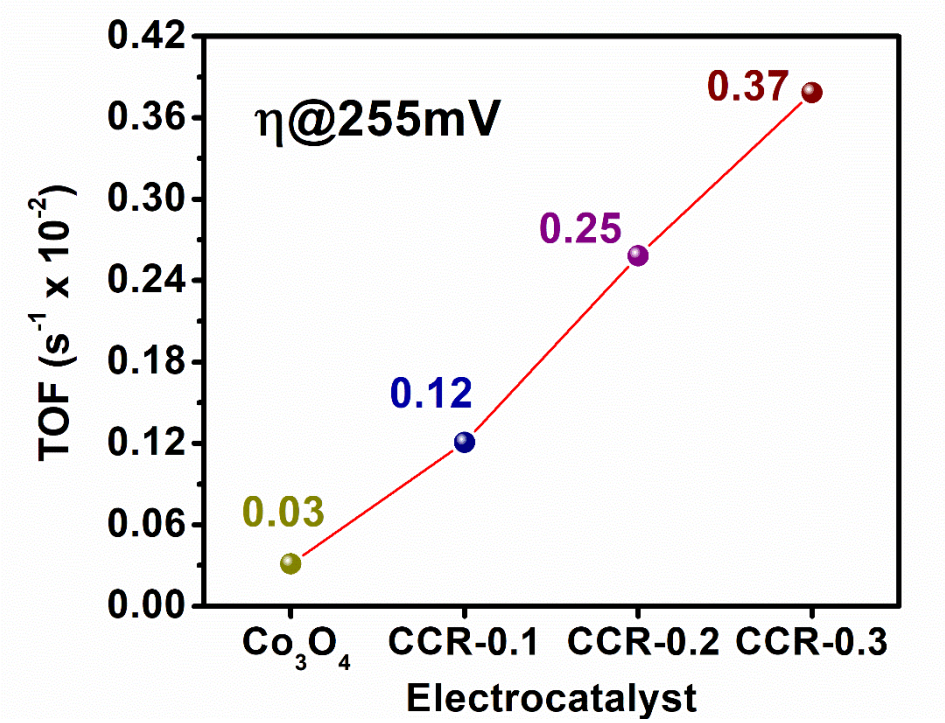

Fig. S9 TOF data of various catalyst at overpotential of 255mV

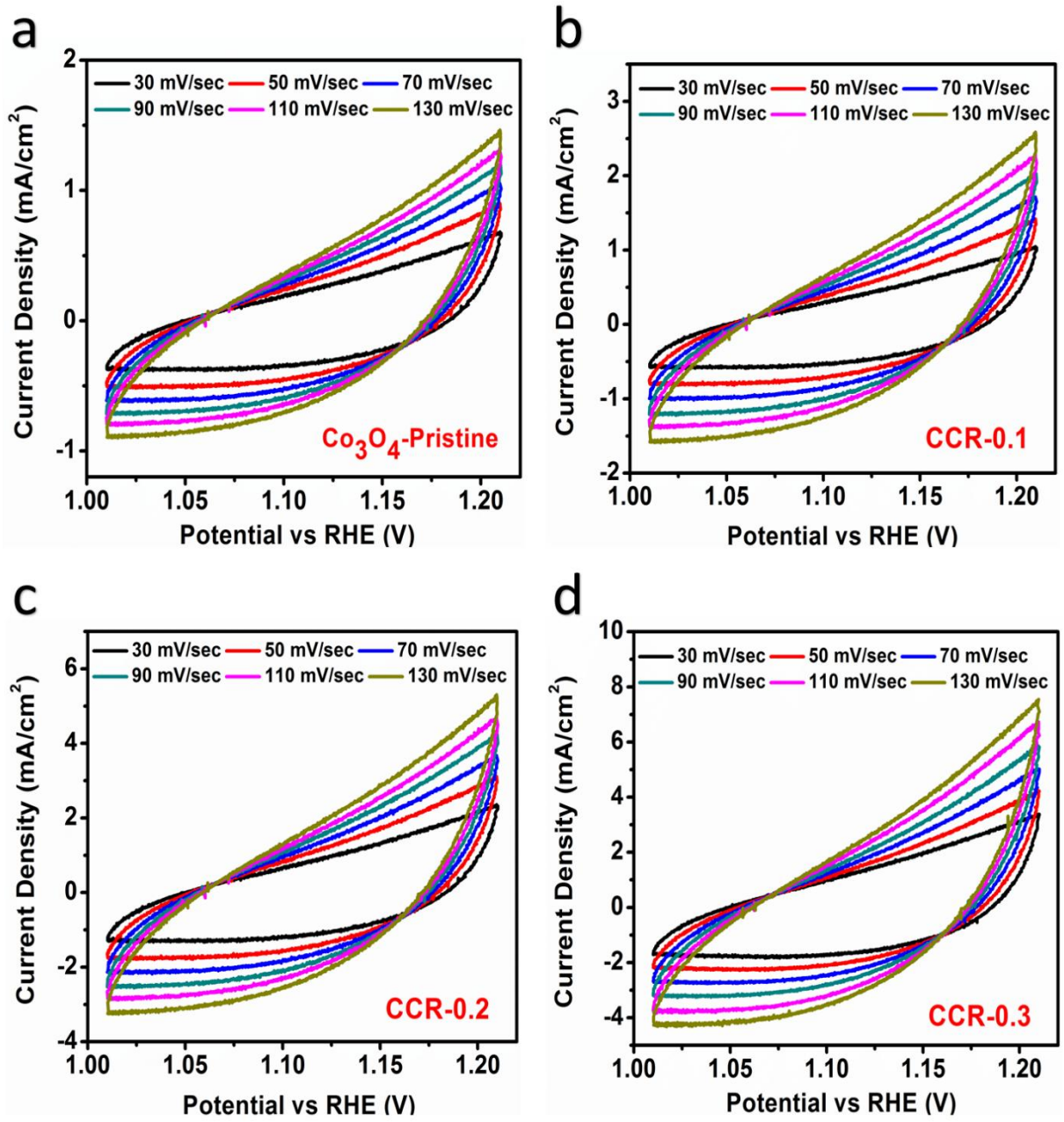

Fig. S10 Cyclic voltametric curves at various scan rate of different catalyst for computation of C_{dl} values.

Table S1. Comparative study of $CrO_{0.87}@Co_3O_4$ composite as OER catalyst with updated electrocatalyst.

Electrocatalyst	**Electrolyte**	**Current Density**	**Overpotential**	**Tafel Slope**	**Ref.**
$CrO_{0.87}@Co_3O_4$	1 M KOH	20 mA cm^{-2}	255 Mv	56 mV dec^{-1}	This work
$Fe_xCo_{3-x}O_4$	3M KOH	10 mA cm^{-2}	266 Mv	52 mV dec^{-1}	[1]
$NiCo_2S_4/C$	1 M KOH	20 mA cm^{-2}	285 mV	61 mV dec^{-1}	[2]
$Mg\text{-}Co_3O_4$	1 M KOH	20 mA cm^{-2}	320 Mv	65 mV dec^{-1}	[3]
$Co_3O_4@Co_3S_4$	0.5 M KOH	20 mA cm^{-2}	376 mV	80 mV dec^{-1}	[4]
$TiO_2\text{-}Co_3O_4$	1 M KOH	10 mA cm^{-2}	270 mV	60 mV dec^{-1}	[5]
Ni- Co_3O_4	1 M KOH	10 mA cm^{-2}	300 mV	82 mV dec^{-1}	[6]
$CdO\text{-}Co_3O_4$	1 M KOH	10 mA cm^{-2}	310 mV	62 mV dec^{-1}	[7]
$CoP_x\text{-}CoO_y$	1 M KOH	10 mA cm^{-2}	322 mV	102 mV dec^{-1}	[8]
Fe_3O_4/Co_3O_4	1 M KOH	10 mA cm^{-2}	370 mV	80 mV dec^{-1}	[9]

References:

[1] Guragain D, Karna S, Choi J, Bhattarai R, Poudel TP, Gupta RK, et al. Electrochemical Performance of Iron-Doped Cobalt Oxide Hierarchical Nanostructure. Processes. 2021;9.

[2] Aftab U, Tahira A, Mazzaro R, Morandi V, Abro MI, Baloch MM, et al. Facile NiCo2S4/C nanocomposite: an efficient material for water oxidation. Tungsten. 2020;2:403-10.

[3] Samo AH, Aftab U, Yameen M, Laghari AJ, Ahmed M, Lakhan MN, et al. MAGNESIUM DOPED COBALT-OXIDE COMPOSITE FOR ACTIVE OXYGEN EVOLUTION REACTION. Journal of Applied and Emerging Sciences. 2021;02:210-6.

[4] Du X, Su H, Zhang X. 3D hierarchical Co3O4@Co3S4 nanoarrays as anode and cathode materials for oxygen evolution reaction and hydrogen evolution reaction. Dalton Transactions. 2018;47:16305-12.

[5] Aftab U, Tahira A, Gradone A, Morandi V, Abro MI, Baloch MM, et al. Two step synthesis of TiO2–Co3O4 composite for efficient oxygen evolution reaction. International Journal of Hydrogen Energy. 2021;46:9110-22.

[6] Bhatti AL, Aftab U, Tahira A, Abro MI, Kashif samoon M, Aghem MH, et al. Facile doping of nickel into Co3O4 nanostructures to make them efficient for catalyzing the oxygen evolution reaction. RSC Advances. 2020;10:12962-9.

[7] Hanan A, Laghari AJ, Solangi MY, Aftab U, Abro MI, Cao D, et al. Cdo/Co3o4 Nanocomposite as an Efficient Electrocatalyst for Oxygen Evolution Reaction in Alkaline Media. International Journal of Engineering Science Technologies. 2022;6:1-10.

[8] Zhou H, Zheng M, Pang H. Synthesis of hollow amorphous cobalt phosphide-cobalt oxide composite with interconnected pores for oxygen evolution reaction. Chemical Engineering Journal. 2021;416:127884.

[9] Bhatti AL, Aftab U, Tahira A, Abro MI, Mari RH, Samoon MK, et al. An Efficient and Functional Fe3O4/Co3O4 Composite for Oxygen Evolution Reaction. Journal of Nanoscience and Nanotechnology. 2021;21:2675-80.